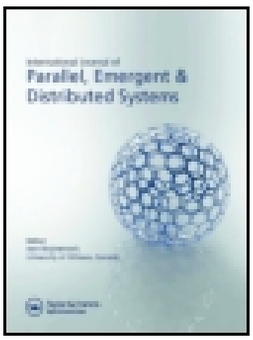

International Journal of Parallel, Emergent and Distributed Systems

ISSN: 1744-5760 (Print) 1744-5779 (Online) Journal homepage: http://www.tandfonline.com/loi/gpaa20

A quantum prisoner's dilemma cellular automaton with probabilistic updating

Ramón Alonso-Sanz

To cite this article: Ramón Alonso-Sanz (2015): A quantum prisoner's dilemma cellular automaton with probabilistic updating, International Journal of Parallel, Emergent and Distributed Systems, DOI: 10.1080/17445760.2015.1096360

To link to this article: http://dx.doi.org/10.1080/17445760.2015.1096360

INTERNATIONAL JOURNAL OF PARALLEL, EMERGENT AND DISTRIBUTED SYSTEMS, 2015
http://dx.doi.org/10.1080/17445760.2015.1096360

Taylor & Francis
Taylor & Francis Group

A quantum prisoner's dilemma cellular automaton with probabilistic updating

Ramón Alonso-Sanz

ETSIA (Estadística, GSC), Technical University of Madrid, C.Universitaria, Madrid, Spain

ABSTRACT

The effect of variable entangling on the dynamics of a spatial quantum formulation of the iterated prisoner's dilemma game is studied in this work. The game is played in the cellular automata manner, i.e. with local and synchronous interaction. The effect of probabilistic updating is assessed in fair and unfair contests, both in the two and three parameter strategy spaces.

ARTICLE HISTORY
Received 16 September 2015
Accepted 16 September 2015

KEYWORDS
Quantum games; entangling; probabilistic; cellular automata

1. The classic and quantum Prisoner's Dilemma

The Prisoner's Dilemma (PD) is a non-zero sum game played by two players, who may choose either to cooperate (*C*) or to defect (*D*). Mutual cooperators each score the *reward R*, mutual defectors score the *punishment P*; *D* scores the *temptation* $\mathfrak{T}$ against *C*, who scores *S* (*sucker*'s payoff) in such an encounter. In the PD it is: $\mathfrak{T} > R > P > S$. The game is symmetric i.e. the payoff matrices of both players are coincident after transposition: $\mathbf{P}_A = \mathbf{P}'_B = \begin{pmatrix} R & S \\ \mathfrak{T} & P \end{pmatrix}$.

1.1. The classic context

In conventional classic games both players decide independently. So that, using uncorrelated probabilistic strategies $\mathbf{x} = (x, 1-x)'$ and $\mathbf{y} = (y, 1-y)'$, the expected payoffs (*p*) in the PD game are:

$$p_A(x,y) = \mathbf{x}'\mathbf{P}_A\mathbf{y} \quad , \quad p_B(x,y) = \mathbf{x}'\mathbf{P}_B\mathbf{y} = \mathbf{y}'\mathbf{P}_A\mathbf{x}. \tag{1}$$

The pair of strategies $(\mathbf{x}, \mathbf{y})$ are in Nash equilibrium (NE) if $\mathbf{x}$ is a best response to $\mathbf{y}$ and $\mathbf{y}$ is a best response to $\mathbf{x}$. Mutual defection, i.e. $\mathbf{x} = \mathbf{y} = (0, 1)$ is the only pair of strategies in NE in the PD game.

In a different game scenario, that of correlated games, an *external* probability distribution $\mathbf{5} = \begin{pmatrix} \pi_{11} & \pi_{12} \\ \pi_{21} & \pi_{22} \end{pmatrix}$ assigns probability to every combination of player choices (23). Thus, the expected payoffs in the PD are:

$$\begin{aligned} p_A &= \pi_{11}R + \pi_{12}S + \pi_{21}\mathfrak{T} + \pi_{22}P \\ p_B &= \pi_{11}R + \pi_{12}\mathfrak{T} + \pi_{21}S + \pi_{22}P. \end{aligned} \tag{2}$$

The quantum game approach described in the next subsection, participates of both the independent players (1) and of the correlated games (2) models.

CONTACT Ramón Alonso-Sanz ramon.alonso@upm.es

1.2. Quantum games

In the quantization scheme introduced by Eisert et al. (12) (EWL for short), the classical pure strategies C and D are assigned two basic vectors $|0\rangle$ and $|1\rangle$ respectively, in a two level Hilbert space. The state of the game is a vector in the tensor product space spanned by the basis vectors $|00\rangle$, $|01\rangle$, $|10\rangle$, $|11\rangle$, where the first and second entries in the ket refer to the players A and B respectively.

The EWL protocol starts with an initial entangled state $|\psi_i\rangle = \hat{J}|00\rangle$, where $\hat{J}$ is a symmetric unitary operator that *entangles* the player's qubits and that is known to both players. To ensure that the classical game is a subset of its quantum version, it is necessary that $\hat{J} = exp\left(i\frac{\gamma}{2}\hat{D}^{\otimes 2}\right) = \cos\left(\frac{\gamma}{2}\right)\hat{I}^{\otimes 2} + i\sin\left(\frac{\gamma}{2}\right)\hat{D}^{\otimes 2}$, with $\hat{D} = \begin{pmatrix} 0 & 1 \\ -1 & 0 \end{pmatrix}$. The *entanglement factor* γ varies in the $[0, \pi/2]$ interval, tuning the degree of entanglement, with $\gamma = 0$ corresponding to the classical (unentangled) game, and $\gamma = \pi/2$ to full entanglement.

The players perform independently their quantum strategies as local unitary operators ($\hat{U}$), $\hat{U}_A$ and $\hat{U}_B$. After the application of these strategies, the state of the game evolves to $|\psi_{f_o}\rangle = (\hat{U}_A \otimes \hat{U}_B)\hat{J}|00\rangle$. Prior to measurement, the $\hat{J}^\dagger$ gate is applied and the state of the game becomes:

$$|\psi_f\rangle = \hat{J}^\dagger(\hat{U}_A \otimes \hat{U}_B)\hat{J}|00\rangle \equiv (\psi_1 \ \psi_2 \ \psi_3 \ \psi_4)' \tag{3}$$

This follows a pair of Stern–Gerlach type detectors for measurement. As a result, $\mathbf{5} = \begin{pmatrix} |\psi_1|^2 & |\psi_2|^2 \\ |\psi_3|^2 & |\psi_4|^2 \end{pmatrix}$. Consequently, the expected payoffs become:

$$\begin{aligned} p_A &= |\psi_1|^2 R + |\psi_2|^2 S + |\psi_3|^2 \mathfrak{T} + |\psi_4|^2 P \\ p_B &= |\psi_1|^2 R + |\psi_2|^2 \mathfrak{T} + |\psi_3|^2 S + |\psi_4|^2 P. \end{aligned} \tag{4}$$

Following the seminal article (12) we will give here consideration first to the two-parameter (2P) subset of the SU(2) space of strategies:

$$\hat{U}(\theta, \alpha) = \begin{pmatrix} e^{i\alpha}\cos(\theta/2) & \sin(\theta/2) \\ -\sin(\theta/2) & e^{-i\alpha}\cos(\theta/2) \end{pmatrix}, \begin{matrix} \theta \in [0, \pi] \\ \alpha \in [0, \pi/2] \end{matrix}. \tag{5}$$

If $\alpha_A = \alpha_B = 0$, or if $\gamma = 0$, the joint probabilities factorize as in the *classical* game employing independent strategies (1) with $x = \cos^2\theta_A/2$, $y = \cos^2\theta_B/2$. So to say, the θ parameters are the *classical* ones. In the classic $\gamma = 0$ context, middle-levels of the θ parameter lead to the equalization of the probabilities in **5**, so that both players get the arithmetic mean of the payoff values.

In contrast, with maximal entangling, if $\theta_A = \theta_B = 0$, a diagonal, i.e. non-factorizable, **5** emerges with $\pi_{11} = \cos^2(\alpha_A + \alpha_B)$, $\pi_{22} = 1 - \pi_{11}$. With maximal entangling, *i*) the equal middle-level election of the parameters by both players leads to a degenerate **5** with $\pi_{22} = 1$. Thus, the 2P model (5) is, so to say, biased towards defection; *ii*) the pair $\{\hat{Q}, \hat{Q}\}$, with $\hat{Q} = \hat{U}(0, \pi/2) = \begin{pmatrix} i & 0 \\ 0 & -i \end{pmatrix}$, is in NE, giving rise to $\pi_{11} = 1$, and in consequence the payoff of mutual cooperation achieved also with the classical strategy $\hat{C} = \hat{U}(0, 0) = I$.

We will consider here also the three-parameter (3P) strategies (7) scenario:

$$\hat{U}(\theta, \alpha, \beta) = \begin{pmatrix} e^{i\alpha}\cos(\theta/2) & e^{i\beta}\sin(\theta/2) \\ -e^{-i\beta}\sin(\theta/2) & e^{-i\alpha}\cos(\theta/2) \end{pmatrix}, \begin{matrix} \theta \in [0, \pi] \\ \alpha, \beta \in [0, \pi/2] \end{matrix}. \tag{6}$$

2. The spatialized quantum PD

In the spatial version of the Quantum PD (QPD) we deal with, each player occupies a site (i, j) in a two-dimensional $N \times N$ lattice. In a cellular automata[1] (CA)-like implementation, in each generation (T)

every player plays with his eight nearest-neighbors and with himself, so that the payoff $p_{i,j}^{(T)}$ of a given individual is the sum over these nine interactions.

In previous studies (5,4), the evolution was guided by the (deterministic) imitation of the best paid neighbour, so that in the next generation, every player will adopt the parameters of his nearest-neighbor (including himself) that received the highest payoff.

In the present study a probabilistic updating mechanism (PCA) is implemented, so that the generic player (i,j) will adopt the parameters of the player (k,l) in his nearest-neighborhood $\mathcal{N}_{(i,j)}$ with probability proportional to his payoff among the payoffs of the neighbors in $\mathcal{N}_{(i,j)}$.

This PCA has been implemented in the classic Battle of the Sexes game (BOS), briefly introduced at the end of this article, played in the CA manner proposed here in (6); but differs from that considered in the study on the evolution of quantum strategies on networks performed in (16) dealing with the PD and other symmetric games.

All the simulations in this work are run in a $N = 200$ lattice with periodic boundary conditions and initial random assignment of the parameter values. The computations have been performed by a double precision Fortran code run on a mainframe.

2.1. Two-parameter strategies

Implementing the two parameter-strategies given in (5) the probability that the player in the cell (i,j) will adopt the parameters of the player (k,l) after the round played at time-step T is:

$$P\left[(\theta_{(i,j)},\alpha_{(i,j)})^{(T+1)} = (\theta_{(k,l)},\alpha_{(k,l)})^{(T)}\right] = \frac{p_{(k,l)}^{(T)}}{\sum\limits_{(i^*j^*)\in\mathcal{N}_{(i,j)}} p_{(i^*j^*)}^{(T)}} \tag{7}$$

Figure 1 deals with the results obtained at $T = 500$ in five simulations (five different initial random assignment of the (θ,α) parameter values) of a two-parameter (5,3,2,1)-QPD PCA with entanglement factor γ. Figure 1 shows in its left frame both the actual mean payoffs ($\overline{p}$) and its mean-field approach (p^*) obtained by using the mean parameter values across the lattice given in the right frame of the figure. Thus, the payoffs achieved in a single hypothetical two-person game with players adopting the mean parameters appearing in the spatial dynamic simulation. Namely,

$$U^* = \begin{pmatrix} e^{i\overline{\alpha}}\cos\overline{\omega} & \sin\overline{\omega} \\ \sin\overline{\omega} & e^{-i\overline{\alpha}}\cos\overline{\omega} \end{pmatrix}$$

The actual and the mean-field payoff fit almost perfectly for low and high γ parameter values, and differ, though not a great extent, in a γ-region characterized below. For low γ-values, the mean payoff is that of the punishment $P = 2$, but a kind of phase-transition appears to happen passed $\pi/8$, so that the reward $R = 3$ is reached before $\pi/4$.

In a conventional (non-CA) QPD game, $\{\hat{D},\hat{D}\}$ are in NE for low values of γ, whereas for high values of the entangling factor, $\{\hat{Q},\hat{Q}\}$ are in NE. The critical values that delimit the NE-regions are: $\gamma^* = \arcsin\left(\sqrt{\frac{P-S}{\mathfrak{T}-S}}\right)$, and $\gamma^\bullet = \arcsin\left(\sqrt{\frac{\mathfrak{T}-R}{\mathfrak{T}-S}}\right)$. If $P - S \leq \mathfrak{T} - R$, i.e. $\gamma^* < \gamma^\bullet$, below γ^*, $\{\hat{D},\hat{D}\}$ are in NE, and over $\gamma^\bullet$, $\{\hat{Q},\hat{Q}\}$ are in NE. In the $(\gamma^*,\gamma^\bullet)$ interval, both $\{\hat{Q},\hat{D}\}$ and $\{\hat{D},\hat{Q}\}$ are in NE (8,10).

The effect of γ in the context of the PCA simulations shown with the (5,3,2,1) PD-parameters of Figure 1 is qualitatively comparable to that just described in the conventional QPD regarding NE: Mutual defection yielding $P = 2$ below $\gamma^* = \arcsin\left(1/2\right) = \pi/6$, $\{\hat{Q},\hat{Q}\}$ yielding $R = 3$ over $\gamma^\bullet = \arcsin\left(1/\sqrt{2}\right) = \frac{\pi}{4}$, and phase-transition in the $(\gamma^*,\gamma^\bullet)$ interval. Such a phase-transition in Figure 1 commences slightly passed γ^* and culminates before $\gamma^\bullet$.

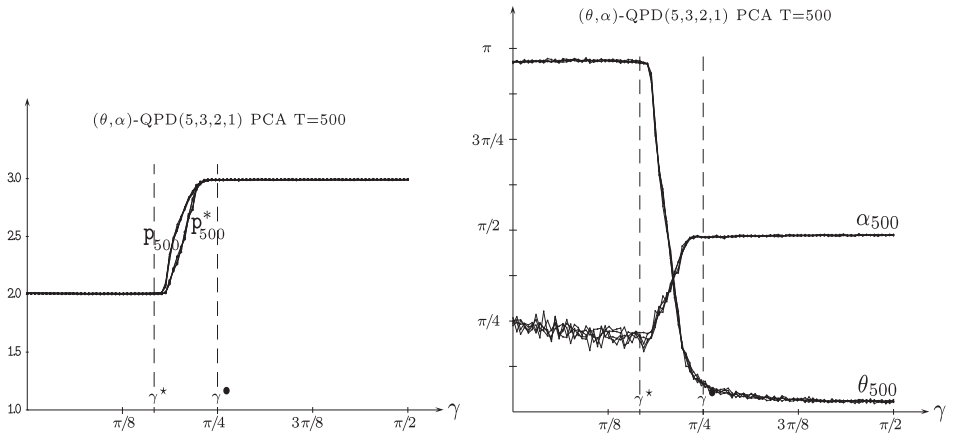

Figure 1. Five simulations at $T = 500$ of a two-parameter (5,3,2,1)-QPD PCA with entanglement factor γ. Left: Actual mean payoffs $\overline{p}$ and mean-field payoffs p^*. Right: Mean parameter values across the lattice.

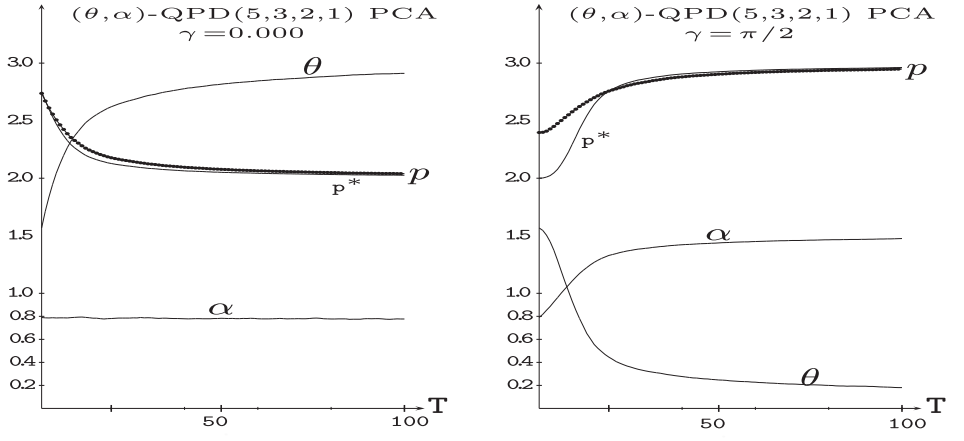

Figure 2. Dynamics up to $T = 100$ in simulations in the two-parameter (5,3,2,1)-QPD PCA scenario of Figure 1. Left: $\gamma = 0$. Right: $\gamma = \pi/2$.

Figure 2 shows the dynamics up to $T = 100$ in simulations in the (5,3,2,1)-QPD PCA scenario of Figure 1 with $\gamma = 0$ (left) and $\gamma = \pi/2$ (right). As a result of the initial random assignment of the parameter values, it is initially in both frames: $\overline{\theta} \simeq \pi/2 = 1.57$, and $\overline{\alpha} \simeq \pi/4 = 0.78$. With $\gamma = 0$, $\overline{\alpha}$ remains unaltered around its initial towards to the $\pi/4$ value, whereas $\overline{\theta}$ rockets towards to the π landmark, i.e. the parameters of the D strategy. With $\gamma = \pi/2$, $\overline{\alpha}$ rockets towards to the $\pi/2$ landmark, and $\overline{\theta}$ plummets to zero, i.e. the parameters of the Q strategy. Please, note that in both cases the tendencies heavily emerge from the very beginning, despite the probabilistic nature of the updating in the CA.

Figure 3 deals with a simulation of a (5,3,2,1)-QPD PCA scenario of Figure 1 for the entanglement factor $\gamma = 0.654$, i.e. in the middle of the $[\gamma^*, \gamma^\bullet]$ transition interval. The far left panel of the figure shows the evolution up to $T = 500$, of the mean values across the lattice of θ, α as well as the actual payoffs ($\overline{p}$) and the mean-field payoffs (p^*). The $\overline{\alpha}$ parameter increases its value in the beginning of the simulation, but by $T = 250$ it has reached a plateau level of approximately 1.1. The $\overline{\theta}$ parameter notably increases its value at the first time-steps, but afterwards it decreases in a monotone way.

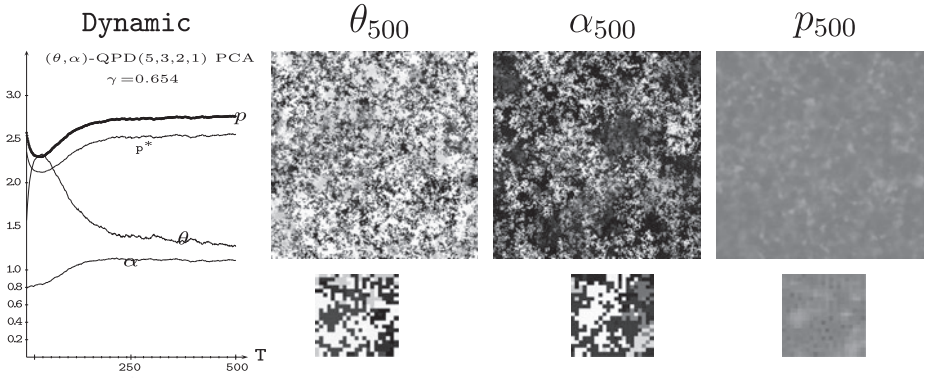

Figure 3. A simulation in the two-parameter (5,3,2,1)-QPD PCA scenario of Figure 1 with $\gamma = 0.654$. Far Left: Evolving mean parameters and payoffs. Center: Parameter patterns at $T = 500$. Far Right: Payoff patterns at $T = 500$. Increasing grey levels indicate increasing parameter values.

Further evolution of this simulation maintains the smooth decrease of $\overline{\theta}$, accompanied by an small increase of $\overline{\alpha}$, so that by $T = 1000$ both parameter values become fairly equal, $\overline{\theta} \simeq \overline{\alpha} = 1.2$.

The actual mean payoff $\overline{p}$ initially decreases its value, in parallel with the increase of $\overline{\theta}$, but soon recovers from the initial small depletion, in parallel with the $\overline{\theta}$ decrease, and becomes fairly stabilized by $T = 300$, with a very smooth further increase. It is $\overline{p} = 2.76$ at $T = 500$ and $\overline{p} = 2.79$ at $T = 1000$. Figure 3 shows also the parameter and payoff patterns at $T = 500$ both for the full lattice and the zoomed 11×11 central part. The parameter patterns show a kind of fine-grain aspect, a kind of spatial heterogeneity that explains why the theoretical mean-field estimations of the payoffs differ from the actual ones, in this particular simulation with p^* below $\overline{p}$. The spatial structures of the parameter and payoff patterns shown in Figure 3 notably differ form that much more uniform patterns achieved with deterministic updating (4,5).

The general form of the plots in Figure 1 remains in CA-simulations with choices of the PD parameters different from that primarily adopted here, i.e. (5,3,2,1). But the details of the transition from *P* to *R* vary notably accordingly to the hierarchy of the γ^* and $\gamma^\bullet$ values. Thus, the order $\gamma^* < \gamma^\bullet$ (that applies with (5,3,2,1)) may be inverted into $\gamma^\bullet < \gamma^*$, in which case, in the $(\gamma^\bullet, \gamma^*)$ interval both $\{\hat{Q}, \hat{Q}\}$ and $\{\hat{D}, \hat{D}\}$ are in NE in conventioal quantum games. In the limit case it is $\gamma^* = \gamma^\bullet$. In these alternative PD-scenarios, the $\overline{p}$-transition from *P* to *R* in CA-simulations occurs abruptly when γ increases. In these alternative PD-parameter scenarios the *P* to *R* transition becomes a kind of phase-transition that has been tested in Figure 4 with the PD-parameters (4,3,2,0), i.e. $\gamma^* = \arcsin(1/2) > \gamma^\bullet = \arcsin(1/\sqrt{2})$ (*P*-marked plots in the right frame of Figure 4), and with (4,3,2,1), i.e. $\gamma^* = \gamma^\bullet = \arcsin(1/2)$ (*P*-marked plots in the left frame of Figure 4). In the former case the abrupt transition from $P = 2$ to $R = 3$ occurs close to the middle of the $(\gamma^\bullet, \gamma^*)$ interval, and in the latter case, as foreseeable, close to $\gamma^* = \gamma^\bullet$. The D-marked plots in both frames of Figure 4 show the transition from $P = 2$ to $R = 3$ with deterministic updating of the strategy parameters. In both scenarios, the transition is more noisy than with probabilistic updating, and occurs at lower γ values, particularly in the $\gamma^* = \gamma^\bullet$ scenario (left frame).

2.2. *Three-parameter strategies*

Implementing the three parameter-strategies given in (6) the formula given in (7) will incorporate the β parameter.

Figure 5 shows the results achieved in the scenario of Figure 1, but in the three-parameter strategies model. At variance with what happens with two parameters (Figure 1), the actual mean payoffs ($\overline{p}$) increase fairly monotonically under the three-parameter strategies model (left frame of Figure 5),

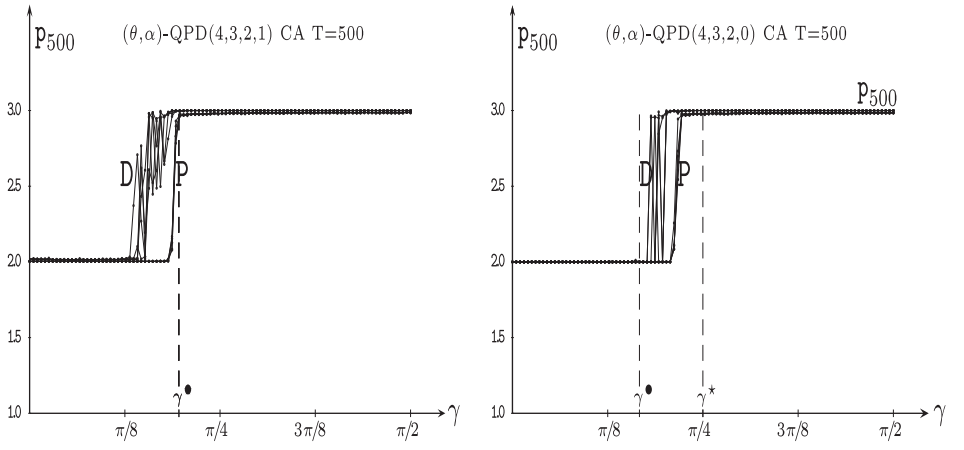

Figure 4. Actual mean payoffs across the lattice ($\overline{p}$) in five simulations at $T = 500$ of two-parameter QPD CA with entanglement factor γ. Left: (4,3,2,1)-PD parameters. Right: (4,3,2,0)-PD parameters. P: Probabilistic updating, D: Deterministic updating.

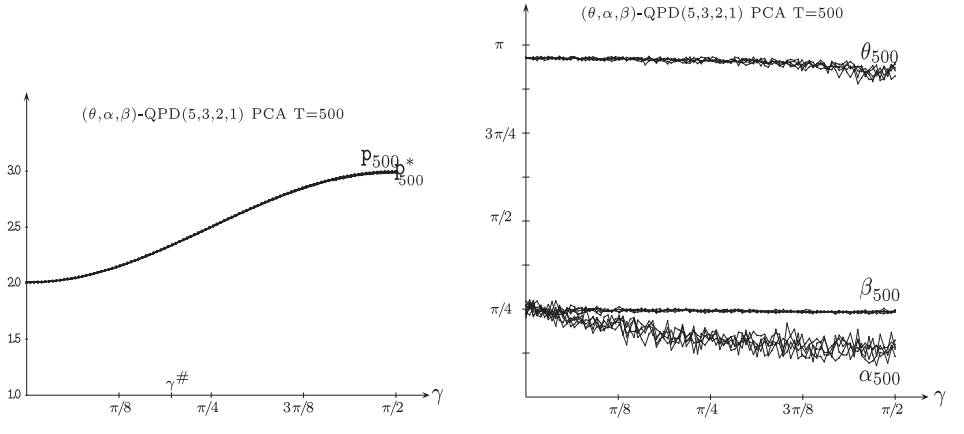

Figure 5. Five simulations at $T = 500$ in a three-parameter (5,3,2,1)-QPD PCA with entanglement factor γ. Left: Actual mean payoffs $\overline{p}$, and mean-field payoffs p^*. Right: Mean parameter values across the lattice.

again, from a mean payoff equal to punishment $P = 2$ up to the reward $R = 3$. The mean-field payoff approach (p^*) fits almost perfectly to the actual payoff ($\overline{p}$).

The right frame of Figure 5 shows that: (i) the $\overline{\beta}$ parameter does not vary appreciably from its initial assignment $\pi/4$, regardless γ, (ii) the $\overline{\theta}$ parameter does not depend very much of γ, reaching values close to π, and (iii) $\overline{\alpha}$ smoothly decreases from $\pi/4$ as γ increases.

No pair of pure strategies in NE exists in the conventional (non-CA) model with three parameters and $\gamma = \pi/2$, but there are an infinite number of mixed strategies in NE (11). In (10)[2] pure strategies in NE are described in the conventional three-parameter scenario below the threshold $\gamma^\# = \arcsin\left(\sqrt{\frac{P-S}{\mathfrak{T}+P-R-S}}\right)$, resulting in the same payoffs for both players : $p^\# = P+(R-P)\sin^2\gamma$.

No discontinuity is apparent at $\gamma^\# = \arcsin(\sqrt{1/3}) = 0.615$ in the CA-simulations in Figure 5. Thus, it is conjecturable that the dynamics in this scenario resorts somehow to the mixed strategies in NE described in (10). In any case, for the (5,3,2,1) PD-parameters in Figure 5, the formula $p^\#(\gamma) = 2+\sin^2\gamma$ is perfectly verified for the actual mean payoffs (and their mean-field approach). Thus for example for

the two extreme values of the entangling factor: $p^{\#}(0) = P = 2$, $p^{\#}(\pi/2) = R = 3$, and fairly for its middle value $p^{\#}(\pi/4) = (P+R)/2 = 2.5$.

The results just reported in Figure 5 apply also to CA-simulations with the $(\gamma^* = \gamma^{\bullet})$-PD-parameters (4,3,2,1), and with the $(\gamma^* > \gamma^{\bullet})$-PD-parameters (4,3,2,0). In these alternative PD-scenarios, the $\overline{\alpha}$ mean parameter remains close to $\pi/4$, as $\overline{\beta}$ does, but no other distinctive effects have been found.

3. Unfair contests

In order to compare different types of players, e.g. here quantum vs. classic, two types of players, termed *A* and *B*, are to be considered. *A* and *B* players alternate in the site occupation in a chessboard form, so that every player is surrounded by four partners (*A*-*B*, *B*-*A*), and four mates (*A*-*A*, *B*-*B*). Again in a CA-like implementation, in each generation (T) every player plays with his four adjacent partners, so that the payoff $p_{i,j}^{(T)}$ of a given individual is the sum over these four interactions. Following the PCA implemented in this study, the generic player (i,j) will adopt the parameters of his mate player (k,l) with a probability proportional to his payoff among their mate neighbors. Thus, the expression (7) still applies, but with $\mathcal{N}_{(i,j)}$ denoting the mate neighborhood of the cell (i,j), not its whole neighborhood.

Let us assume the unfair situation: A type of players is restricted to classical strategies $\tilde{U}(\theta,0)$, whereas the other type of players may use quantum $\hat{U}(\theta,\alpha)$ ones (13).

Figure 6 shows the asymptotic payoffs in five simulations of an unfair quantum two-parameter (5,3,2,1)-PD PCA with variable entanglement factor γ. The behavior for low and high values of the entanglement factor is somehow that expected: with low values of γ the asymptotic payoff maintain the $P = 2$ punishment value, and with $\gamma > \pi/4$ the payoff of the quantum players (red-marked) out scores that of the classic player (blue-marked). But, what happens in the $(\gamma^*, \gamma^{\bullet}) = (0.524, \pi/4)$ interval is highly unexpected: the classic player out scores the quantum player. The peak emerging just after $\gamma^* = 0.524$ in particular is extremely surprising. For γ increasing from this value, up to $\gamma^{\bullet} = \pi/4$, the inversion in the ordering of the payoffs in depleted, up to reaching the same *p*-value, the reward $R = 3$, by $\gamma^{\bullet} = \pi/4$. It seems that the bias towards defection referred in the Section 1.2 overcomes the fact that the $\mathbb{A}$ player is a quantum player when entangling commences to operate but remains below its middle level. After the $\gamma^{\bullet}$ value, the expected ordering of the $\overline{p}$'s slowly appears, with a sort of noisy behaviour appearing after $\gamma = (\pi/4 + 3\pi/8)/2$. This discontinuity refers not only to the breaking of the increasing quantum over classic tendency, but also to the fact that the five different simulations become appreciable. It is remarkable that, with this exception, the *p*-values in the five simulations fairly coincide, also in the peak of the classic player.

Figure 7 shows the mean parameters and its corresponding payoffs in the unfair quantum two-parameter (red) vs. classic (blue) scenario of Figure 6. The curves labelled p^* in the right panel of Figure 7 show the mean-field payoffs of both players, i.e. the payoffs achieved in a single hypothetical two-person game with players adopting the mean parameters appearing in the spatial dynamic simulation, given in the right panel of Figure 7. Namely,

$$U_{\mathbb{A}}^{*} = \begin{pmatrix} e^{i\overline{\alpha}_{\mathbb{A}}}\cos\overline{\omega}_{\mathbb{A}} & \sin\overline{\omega}_{\mathbb{A}} \\ \sin\overline{\omega}_{\mathbb{A}} & e^{-i\overline{\alpha}_{\mathbb{A}}}\cos\overline{\omega}_{\mathbb{A}} \end{pmatrix} \quad , \quad U_{\mathbb{B}}^{*} = \begin{pmatrix} e^{i\overline{\alpha}_{\mathbb{B}}}\cos\overline{\omega}_{\mathbb{B}} & \sin\overline{\omega}_{\mathbb{B}} \\ \sin\overline{\omega}_{\mathbb{B}} & e^{-i\overline{\alpha}_{\mathbb{B}}}\cos\overline{\omega}_{\mathbb{B}} \end{pmatrix}.$$

The mean-field payoffs estimations given in the right frame of Figure 7 fit fairly well to the actual ones shown in Figure 6 for not too high values of γ. But when γ approaches $3\pi/8$ the p^* values notably differ from the $\overline{p}$ ones. This fact will be commented below, when dealing with Figure 8.

In a conventional (non CA) unfair 2P QPD game, the quantum player is well advised to play the *miracle* strategy $\hat{M} = \hat{U}(\pi/2, \pi/2) = \frac{1}{\sqrt{2}}\begin{pmatrix} i & 1 \\ -1 & -i \end{pmatrix}$ (12). Provided that $\gamma > \pi/4$, the strategy $\hat{M}$ ensures to the quantum player to over-rate the classic player, even if the classic player chooses $\hat{D}$. Inthe case

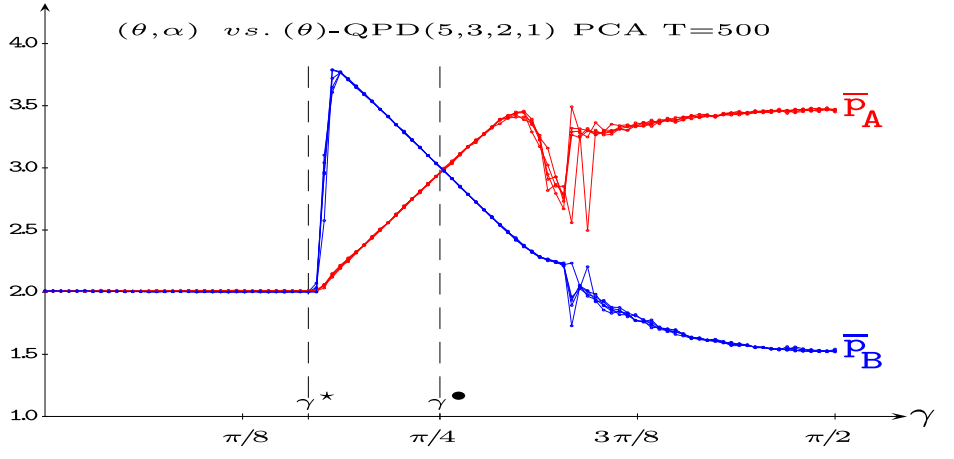

Figure 6. Asymptotic payoffs in five simulations of an unfair quantum two-parameter (red) vs. classic (blue) (5,3,2,1)-PD PCA with variable entanglement factor γ.

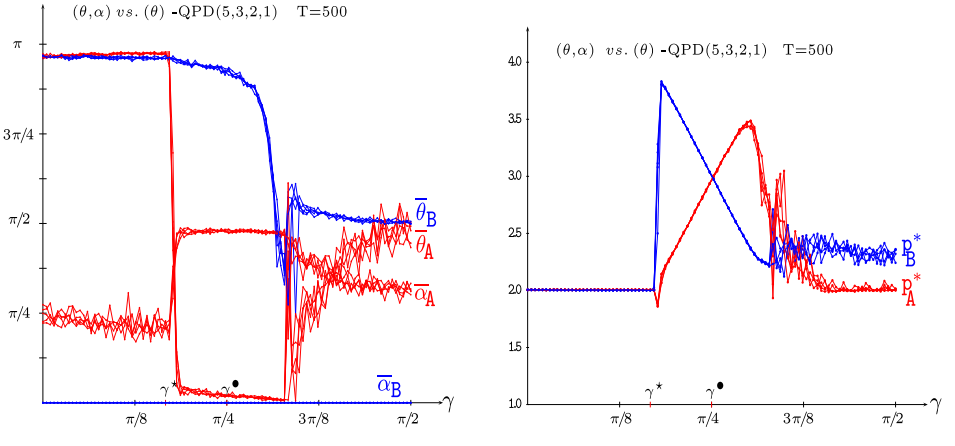

Figure 7. Mean parameters and its corresponding payoffs in the unfair quantum two-parameter (red) vs. classic (blue) scenario of Figure 6.

of full entangling, $\hat{M}$ vs. $\hat{D}$ will provide the payoff $\frac{\mathfrak{T}+P}{2}$ to the quantum player, whereas the classic player will get $\frac{S+P}{2}$. In the context of Figure 6 it is: $\frac{\mathfrak{T}+P}{2}=3.5$, and $\frac{S+P}{2}=1.5$, numerical values of the payoffs close to those achieved by the $\overline{p}$ values for $\gamma=\pi/2$ in Figure 7.

Figure 8 deals with a simulation in the $\gamma=\pi/2$ unfair scenario of Figure 6: A (5,3,2,1)-PD PCA where the B players (blue) are restricted to classical strategies, i.e. $\alpha_{\mathrm{B}}=0$. The far left panel of the figure shows the evolution up to T=500 of the mean values across the lattice of θ,α as well of the actual and theoretical mean payoffs. Both figures shows also the snapshots of the parameter and payoff patterns at $T=500$, both for the full lattice and the zoomed central part. As a result of the random assignment of the parameter values it is initially: $\overline{\theta}_{\mathrm{A}}\simeq\overline{\theta}_{\mathrm{B}}\simeq\pi/2=1.57$, and $\overline{\alpha}_{\mathrm{A}}\simeq\overline{\alpha}_{\mathrm{B}}\simeq\pi/4=0.78$.

The parameter patterns in Figure 8 show a kind of coarse-grain aspect, a kind of spatial heterogeneity that explains why the theoretical mean-field estimations of the payoffs very much differ from the actual ones, in this particular case even inverting the order of magnitude, i.e. $\overline{p}_{\mathrm{A}}>\overline{p}_{\mathrm{B}}$, but $p^*_{\mathrm{A}}<\overline{p}_{\mathrm{B}}$. The spatial structures of the parameter and payoff patterns here obtained with probabilistic CA-updating

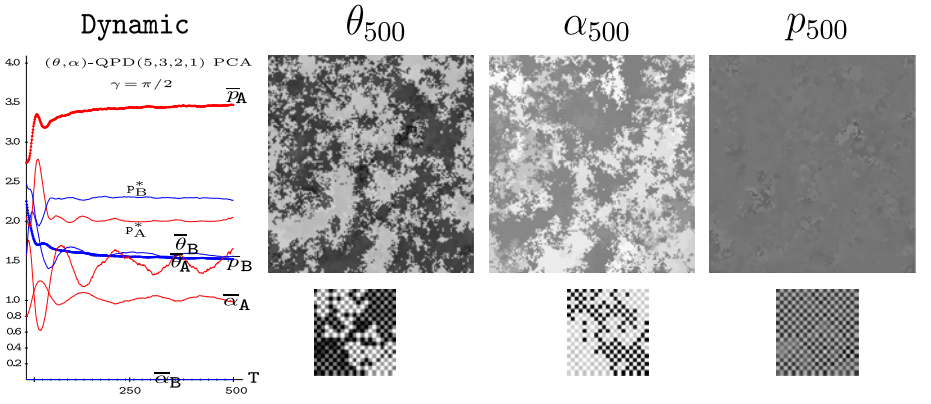

Figure 8. A simulation in the $\gamma = \pi/2$ unfair scenario of Figure 6. Far Left: Evolving mean parameters and payoffs. Center: Parameter patterns. Far Right: Payoff patterns. Increasing grey levels indicate increasing parameter values.

differ very much form that achieved with deterministic updating (5,4), in which case rich maze like patterns emerge.

The trait features of the graphs in Figure 6 are preserved in CA-simulations with the ($\gamma^* = \gamma^\bullet$)-PD-parameters (4,3,2,1). With the ($\gamma^* > \gamma^\bullet$)-PD-parameters (4,3,2,0), the actual $\overline{p} = P = 2$ remains stable for both types of players up to $\gamma^* = \pi/4$, at this value of γ a crisp bifurcation emerges, so that at $\gamma = \pi/2$ it is $\overline{p}_A = 3.0$ and $\overline{p}_B = 1.0$.

3.1. Unfair three-parameter contests

Figure 9 shows the asymptotic payoffs in five simulations of an unfair quantum three-parameter (5,3,2,1)-PD CA with variable entanglement factor γ. The general features of Figure 6 participates of the trait features of the plots in Figure 5 and in Figure 6. Thus, for low values of γ the actual mean payoffs of both types of players evolve as in Figure 5: Up to $\gamma = \gamma^*$ they coincide and increase its value smoothly, following the formula $p^\#(\gamma) = 2 + \sin^2(\gamma)$. In the ($\gamma^*, \gamma^\#$) interval the quantum player slightly over-rates the classic player, but by $\gamma = \gamma^\#$ both mean payoffs $\overline{p}$ diverge as in Figure 6: The classic player over-rates the quantum player in the ($\gamma^\#, \gamma^\bullet$) interval, equalization achieved at level $\overline{p} = R = 3$ for $\gamma = \gamma^\bullet$, and $\overline{p}_A > \overline{p}_B$ for $\gamma > \gamma^\bullet$. The interval of γ for which the classic player over-rates the quantum player is narrower in Figure 9 compared to that in Figure 6: ($\gamma^\#, \gamma^\bullet$) instead of ($\gamma^*, \gamma^\bullet$), with the classic player reaching a lower peak in his payoff. In Figures 9 and 6 roughly the same $\overline{p}$-values are achieved by $\gamma = \pi/2$: $\overline{p}_A = 3.5$, $\overline{p}_B = 1.5$.

The mean-field payoffs in the scenario of Figure 9, shown in the right frame of Figure 10, prove the existence of heavy spatial effects for high values of γ: The mean-field payoffs are far distant of the actual mean payoffs, and with their ordering inverted.

The trait features of the graphs in Figure 9 are preserved in CA-simulations with the PD-parameters (4,3,2,1), though with equal mean payoffs for both players reaching $\gamma = \gamma^\# > \gamma^\bullet = \gamma^*$. With the ($\gamma^* > \gamma^\bullet$)-PD-parameters (4,3,2,0), equal mean payoffs remain up to approximately the center of the ($\gamma^*, \gamma^\#$) interval. In these scenarios, a fairly crisp bifurcation of the $\overline{p}$'s actual payoffs emerges after the equal $\overline{p}'s$ behaviour, with a minimum γ interval in which the classic player over-rates the quantum player.

The plots in the simulations of an unfair quantum vs. (θ, α)-semi-quantum three-parameter (5,3,2,1)-PD CA shown in Figure 11 preserve the trait features of those in Figure 9, except in what respect to the tendency to equalization of the payoff of both types of players for the highest values of γ.

The mean-field payoffs in the scenario Figure 11, shown in the right frame of Figure 12, prove the existence of huge spatial effects for high values of γ: The mean-field payoffs rocket towards the extreme values (5,1), far distant of the actual mean payoffs. The discrepancy between the actual and

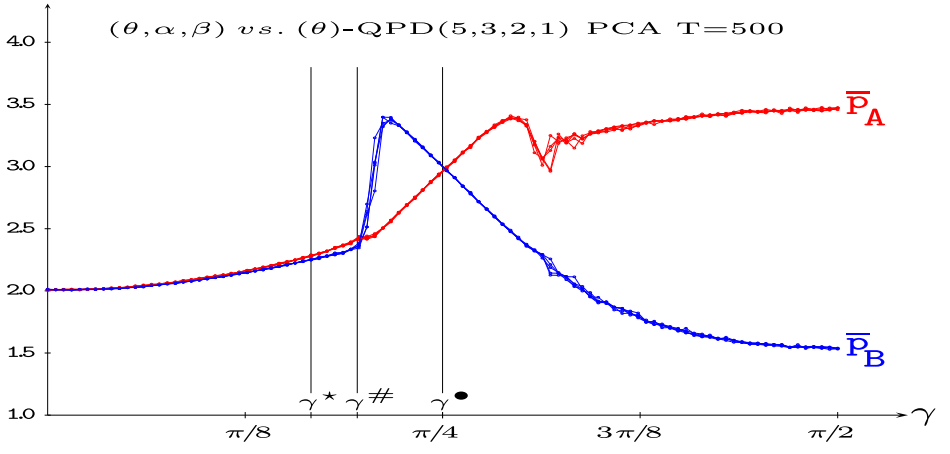

Figure 9. Asymptotic payoffs in five simulations of an unfair three-parameter quantum (red) vs. classic (blue) (5,3,2,1)-PD PCA with entanglement factor γ.

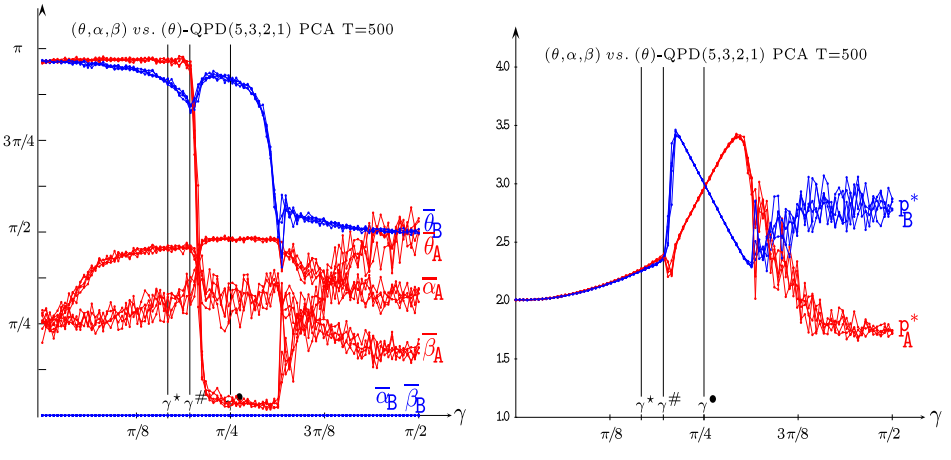

Figure 10. Mean parameters and its corresponding payoffs in the unfair quantum three-parameter (red) vs. classic (blue) scenario of Figure 9.

the mean-field payoffs is still found with the (4,3,2,1)-PD parameters, but not with the (4,3,2,0)-PD parameters.

In the unfair quantum vs. (θ,β)-semi-quantum simulations shown in Figure 13 the plots appearance surprisingly looks-like that in Figure 5. Only a minor discrepancy between the actual mean payoffs and its mean-field approach may be appreciated in the left frame of Figure 13 for high values of γ.

The (θ,β) parameterization considered in Figure 13 was implemented in (9) and studied in (14) with strategies of the form: $\hat{U}(\theta,\beta)=\begin{pmatrix}\cos(\theta/2) & ie^{i\beta}\sin(\theta/2)\\ ie^{-i\beta}\sin(\theta/2) & \cos(\theta/2)\end{pmatrix}$. In (14) it is reported that in conventional (non-CA) (θ,β) EWL models with (5,3,1,0) PD-parameters, the pair $\{\hat{D}',\hat{D}'\}$, $\hat{D}'=\frac{1}{\sqrt{2}}\begin{pmatrix}0 & i-1\\ i+1 & 0\end{pmatrix}$, is in Nash equilibrium for all γ with equal payoffs for both players: $p_A=p_B=1+2\sin^2\gamma$, whose form is reminiscent of that of the plots in Figure 13.

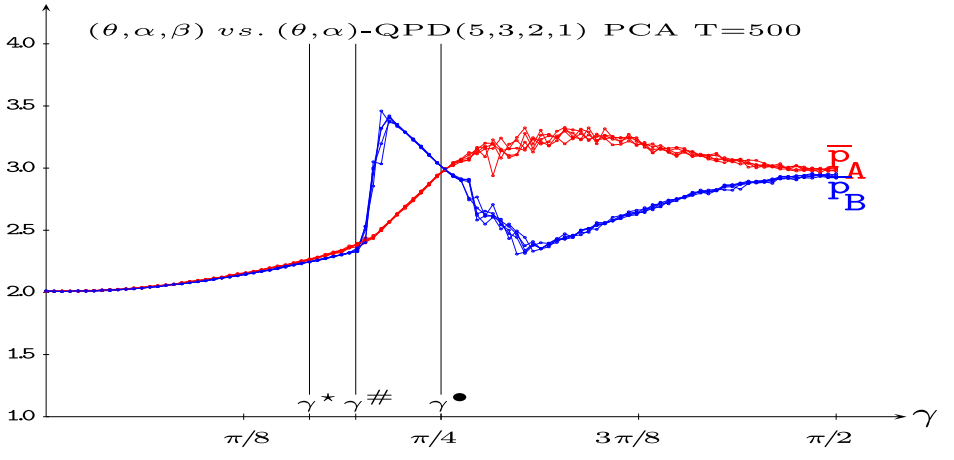

Figure 11. Asymptotic payoffs in five simulations of an unfair three-parameter quantum (red) vs. (θ,α)-semi-quantum (blue) (5,3,2,1)-PD PCA with entanglement factor γ.

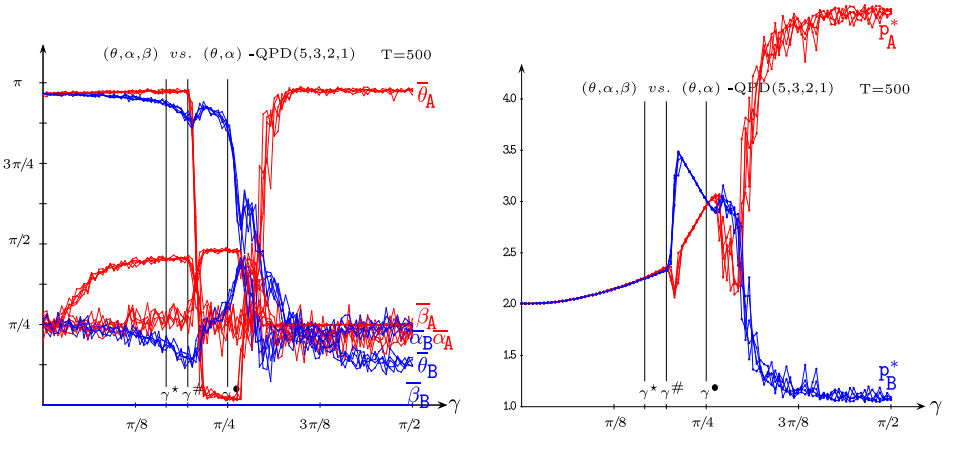

Figure 12. Mean parameters and its corresponding payoffs in the unfair quantum three-parameter (red) vs. (θ,α)-semi-quantum (blue) scenario of Figure 11.

The trait features of the plots in Figure 13 remain unchanged with the choices (4,3,2,1) and (4,3,2,0) of the PD parameters.

3.2. A note on the QBOS PCA game

The so called BOS is a simple example of a two-person (♀ and ♂), non-zero sum asymmetric game, i.e. a game whose payoff matrices are not coincident after transposition. Thus, for example: $\mathbf{P}_{♂} = \begin{pmatrix} R & 0 \\ 0 & r \end{pmatrix}$, and $\mathbf{P}_{♀} = \begin{pmatrix} r & 0 \\ 0 & R \end{pmatrix}$. The payoffs $R > r > 0$ quantify the preferences of both players. Thus, in the BOS game both players hope to *coordinate* their choices, but the *conflict* is also present because their preferred choices differ (23). In CA-simulations of asymmetric games (3,2), the distinction between two types of players is mandatory, not only an artefact to allow comparisons of players with different capabilities, as done here when dealing with unfair games.

In the studies (3,2) the unfair contest of the type quantum-male vs. classic-female was considered. At variance here, the unfair contest: classic-male vs. quantum-female is taken into account. Thus,

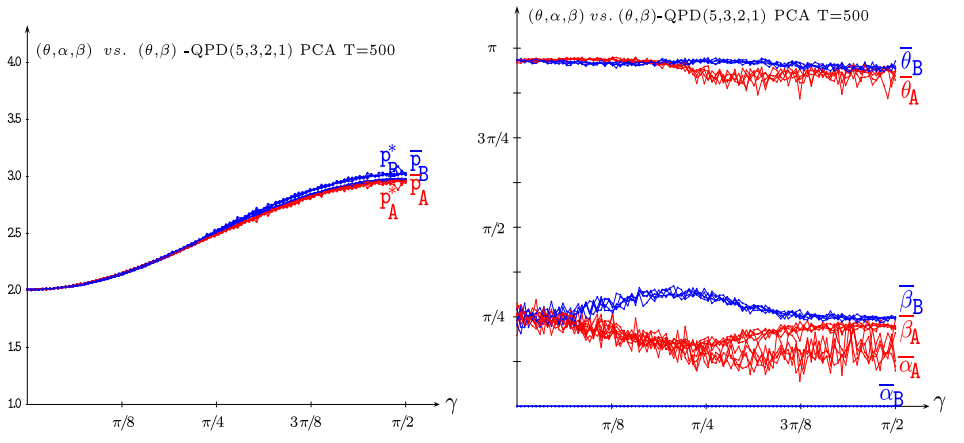

Figure 13. Five simulations at $T = 500$ in an unfair three-parameter quantum (red) vs. (θ, β)-semi-quantum (blue) (5,3,2,1)-PD PCA with entanglement factor γ. Left: Actual mean payoffs $\overline{p}$ and mean-field payoffs p^*. Right: Mean parameter values across the lattice.

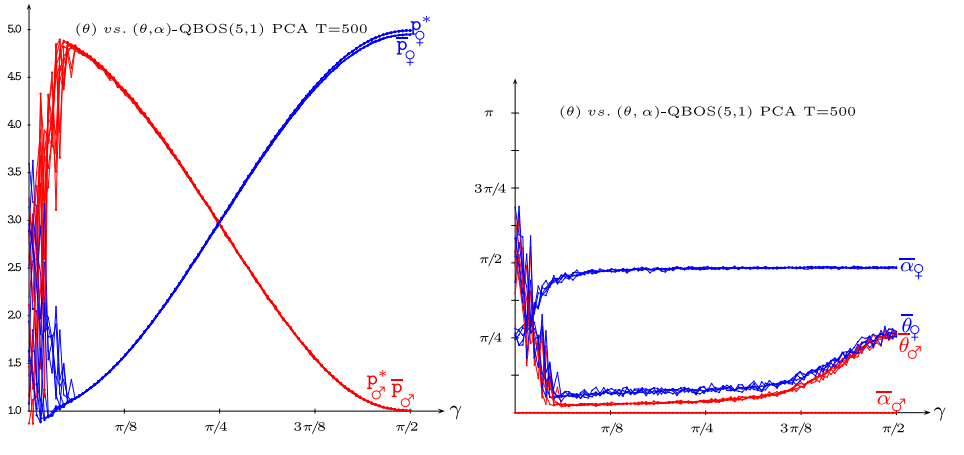

Figure 14. Five simulations at $T = 500$ of an unfair classic male (red) vs. a two-parameter quantum female (red) in a (5,1)-QBOS PCA with entanglement factor γ. Left: Actual mean payoffs ($\overline{p}$) and mean-field payoffs (p^*). Right: Mean parameter values across the lattice.

Figure 14 deals with five simulations at $T = 500$ of an unfair two-parameter classic male (red) vs. quantum male (blue) in a (5,1)-QBOS PCA with entanglement factor γ. In the left frame the actual mean payoffs ($\overline{p}$), and the mean-field payoffs (p^*) are shown. The right frame shows the parameter values across the lattice of both types of players. In the quantum-male vs. classic-female studied before (3,2), the quantum-male over rates the quantum-female in a very clear way as soon as the γ factor takes off. At variance here, Figure 14 shows a more variable dependence of γ, with $\gamma = \pi/4$ marking the turning point for the quantum female player over scoring the classic male player. Also remarkable in Figure 14 is the perfect fit of the mean-field payoffs (p^*) to the actual mean payoffs ($\overline{p}$) as soon as γ takes off.

4. Conclusions and future work

A spatial formulation of the iterated QPD game with arbitrary entangling is studied in this work. The game is played in the cellular automata (CA) manner, i.e. with local and synchronous players interaction. The evolution is achieved via probabilistic imitation of the neighbours.

In fair quantum vs. quantum contests, it is shown how increasing entangling supports the increasing of the mean payoff across the lattice, from the punishment (the second lowest PD-parameter) with no entangling, up to the reward (the second highest PD-parameter) with maximal entangling. This transition is fairly smooth in the with players implementing three-parameter strategies, whereas a kind of phase transition emerges in the two-parameter strategies context.

In the unfair quantum vs. classic scenario, the effect of entangling appears to be much more complex. Thus, above a landmark level of entangling, the quantum player over scores the classic player, but for levels of the entangling factor below but close to this landmark entangling, unexpectedly the classic player over scores the quantum player.

Mean-field approaches of the actual mean payoffs across the lattice (obtained by using the mean parameter values across the lattice) fit fairly well in most of the scenarios studied in this article. But in some cases, particularly when dealing with unfair games, spatial effects emerge so that the mean-field analysis fails to approach the actual mean payoffs.

Other quantization schemes (21,22) deserve particular studies in the spatial context. In particular the scheme introduced by Marinatto and Weber (19), in which the bias to defection is avoided by stating the initial state of the game $|\psi_i\rangle$ as a linear combination of the vectors of the base ($|00\rangle$, $|01\rangle$, $|10\rangle$, $|11\rangle$), and also differs from the seminal model proposed of Eisert et al. (12) by the absence of the reverse gate $J^\dagger$.

Further study is due on structurally dynamic quantum games, in games with asynchronous updating, as well as on the effect of increasing degrees of spatial dismantling. These are deviations from the canonical cellular automata paradigm which may lead to more realistic models. Particularly, with embedded tuneable memory of past payoffs and parameter values (1).

Notes

1. Cellular automata are spatially extended dynamical systems that are discrete in all their constitutional components: space, time and state-variable. Uniform, local and synchronous interactions, as assumed here, are landmark features of CA (24). Spatialized quantum games are fairly unexplored, even in its simplest form, i.e. in the CA manner considered here. To the best of our knowledge, only the reference (20) may by properly cited in this respect, as the articles (18,17,16,15) are intended in *networks*, not in spatially structured *lattices*.
2. The reference (14) is also relevant at this respect, but the occasional reader should be warned about the variation of the α and β parameters in the $[-\pi,\pi]$ interval instead of in $[0,\pi/2]$, as proposed for α in the seminal EWL paper.

Disclosure statement

No potential conflict of interest was reported by the author.

Funding

This work was supported by the Spanish [grant number M2012-39101-C02-01]. Part of the computations of this work were performed in EOLO and FISWULF, HPC machines of the International Campus of Excellence of Moncloa, funded by the Spanish Government and Feder Funds.

References

[1] R. Alonso-Sanz, Dynamical Systems with Memory, World Scientific Publishing, Singapore, 2011.
[2] R. Alonso-Sanz, *A quantum battle of the sexes cellular automaton*, Proc. R. Soc. A 468 (2012), pp. 3370–3383.
[3] R. Alonso-Sanz, *On a three-parameter quantum battle of the sexes cellular automaton*, Quant. Inform. Process. 12(5) (2013), pp. 1835–1850.
[4] R. Alonso-Sanz, *A quantum prisoner's dilemma cellular automaton*, Proc. R. Soc. A 470 (2014), 9 pages.
[5] R. Alonso-Sanz, *Variable entangling in a quantum prisoner's dilemma cellular automaton*, Quant. Inform. Process. 14(1) (2015), pp. 147–164.
[6] R. Alonso-Sanz, *Self-organization in the spatial battle of the sexes with probabilistic updating*, Physica A 390 (2011), pp. 2956–2967.

[7] S.C. Benjamin and P.M. Hayden, *Comment on 'Quantum games and quantum strategies'*, Phys. Rev. Lett. 87(6) (2001), p. 069801.
[8] J.F. Du, X.D. Xu, H. Li, X. Zhou, and R. Han, *Entanglement playing a dominating role in quantum games*, Phys. Lett. A 89(1–2) (2001), pp. 9–15.
[9] J.F. Du, X.D. Xu, H. Li, X. Zhou, and R. Han, *Entanglement enhanced multiplayer quantum games*, Phys. Lett. A 302 (2002), pp. 222–233.
[10] J.F. Du, H. Li, X.D. Xu, X. Zhou, and R. Han, *Phase-transition-like behaviour of quantum games*, J. Phys. A: Math. Gen. 36(23) (2003), pp. 6551–6562.
[11] J. Eisert and M. Wilkens, *Quantum Games*, J. Mod. Opt. 47(14–15) (2000), pp. 2543–2556.
[12] J. Eisert, M. Wilkens, and M. Lewenstein, *Quantum games and quantum strategies*, Phys. Rev. Lett. 83(15) (1999), pp. 3077–3080.
[13] A.P. Flitney and D. Abbott, *Advantage of a quantum player over a classical one in 2x2 quantum games*, Proc. R. Soc. Lond. A 459(2038) (2003), pp. 2463–2474.
[14] A.P. Flitney and L.C.L. Hollenberg, *Nash equilibria in quantum games with generalized two-parameter strategies*, Phys. Lett. A 363 (2007), pp. 381–388.
[15] Q. Li, A. Iqbal, M. Chen, and D. Abbott, *Evolution of quantum and classical strategies on networks by group interactions*, New J. Phys. 14(10) (2012), 13 pages.
[16] Q. Li, A. Iqbal, M. Chen, and D. Abbott, *Quantum strategies win in a defector-dominated population*, Physica A 391 (2012), pp. 3316–3322.
[17] Q. Li, A. Iqbal, M. Perc, M. Chen, and D. Abbott, *Coevolution of quantum and classical strategies on evolving random networks*, PloS one 8(7) (2013), 10 pages.
[18] A. Li and X. Yong, *Entanglement guarantees emergence of cooperation in quantum Prisoner's Dilemma games on networks*, Sci. Rep. 4 (2014), 7 pages. doi:10.1038/srep06286.
[19] L. Marinatto and T. Weber, *A quantum approach to static games of complete information*, Phys. Lett. A 272 (2000), pp. 291–303.
[20] J.A. Miszczak, L. Pawela, and J. Sladkowski, *General model for an entanglement-enhanced composed quantum game on a two-dimensional lattice*, Fluct. Noise Lett. 13(2) (2014), pp. 1450012. Available at http://arxiv.org/abs/1306.4506.
[21] A. Nawaz and A.H. Toor, *Dilemma and quantum battle of sexes*, J. Phys. A: Math. Gen. 37(15) (2004), pp. 4437–4443.
[22] A. Nawaz and A.H. Toor, *Generalized quantization scheme for two-person non-zero sum games*, J. Phys. A: Math. Gen. 37(42) (2004), pp. 11457–11463.
[23] G. Owen, *Game Theory*, Academic Press, London, 1995.
[24] J.L. Schiff, *Cellular Automata: A Discrete View of the World*, Wiley, Bingley, 2008.